Inclusions in wrought superalloys: a review

Shu-feng Yang[1] · Shu-lei Yang[1] · Jing-long Qu[2] · Jin-hui Du[2] · Yu Gu[2] · Peng Zhao[1] · Ning Wang[1]

Abstract

Inclusions in wrought superalloys significantly affect the stability of the alloy properties and limit their use and development in aeroengines and other applications. The types and sources of inclusions in wrought superalloys were reviewed with analysis of the conditions of inclusion formation from the viewpoints of thermodynamics and kinetics. The thermodynamic data for inclusion formation in nickel-based and cobalt-based alloys were summarized and improved. The damage of inclusions to the fatigue and tensile properties and workability of these alloys and the mechanisms of crack initiation and propagation caused by inclusions were also discussed, and the effects of inclusions with different characteristics on crack propagation were reviewed. In addition, the control methods and mechanisms of inclusions in the triple smelting process (vacuum induction melting + protective electroslag remelting + vacuum arc remelting) were covered, providing a reference for improving the control technology of inclusions in wrought superalloys. Finally, the difficulties and development trends for inclusion control in wrought superalloys were discussed.

Keywords Wrought superalloy · Triple smelting · Inclusion · Control method

1 Introduction

Wrought superalloys are widely used in gas turbines, rocket engines, nuclear reactors, and other applications because of their excellent oxidation resistance, low cycle fatigue, and creep resistance. They are the key materials used in the development and production of new aeroengines in China [1, 2]. With the development of aeroengines with high thrust-to-weight ratio, high efficiency, and high safety, higher requirements have been placed on the quality and performance of wrought superalloys. Inclusions result in the formation of cracks, holes, dirty white spots, and other defects in wrought superalloys [3], leading to deterioration of the service life and mechanical properties of the alloys and reduction of the yield of the alloys and limiting the development of high-performance wrought superalloys in China.

The preparation of wrought superalloy components usually requires smelting, opening, forging, heat treatment, machining, and non-destructive testing [4, 5]. Inclusion generation and removal mainly occur during the smelting process. If the inclusion content of the smelting ingot exceeds the standard, high-performance alloy products cannot be prepared [6]. In the 1980s and 1990s, extensive international research was performed on the precipitation and removal of inclusions in wrought superalloys [7–10]. Recently, with the improvement of China's smelting process, especially the gradual advance of the triple smelting process (vacuum induction melting + protective electroslag remelting + vacuum arc remelting), the content of impurities and inclusions in wrought superalloys has been reduced to a relatively low level [11]. However, compared with wrought superalloys produced internationally, unstable production process, high inclusion content, metallurgical defects, and other problems are still prominent in China [6], and improvement of the cleanliness level of wrought superalloys relying on equipment optimization has reached a bottleneck.

Therefore, a comprehensive understanding of the hazards, formation, and removal mechanism of inclusions in wrought superalloys is of great significance for the preparation of "zero-inclusion wrought superalloys" in China.

✉ Shu-feng Yang
yangshufeng@ustb.edu.cn

1 School of Metallurgical and Ecological Engineering, University of Science and Technology Beijing, Beijing 100083, China

2 Gaona Aero Material Co., Ltd., Beijing 100081, China

2 Hazards of inclusions in wrought superalloys

Because of the special applications of superalloys, their products have extremely strict requirements for the alloy properties [4, 12, 13]. The great differences in the elastic modulus, deformation capacity, and high-temperature oxidation resistance of the inclusions and matrix [14, 15] seriously affect the mechanical and processing properties of superalloys. In 2016, the high-pressure turbine disk on the US B767-300 aircraft failed at Chicago O'Hare International Airport [16]. The investigation indicated that the Al_2O_3–MgO–TiN inclusion cluster in Inconel 718 alloy used in the turbine disk became the initiation site of a fatigue crack, which caused the accident, as shown in Fig. 1 [16]. This example directly demonstrates that inclusions can be very harmful to the properties of alloys. This section summarizes the relevant studies on the effect mechanism of inclusions on the tensile, fatigue, and machining properties of wrought superalloys and provides references for further understanding of the hazards of inclusions.

2.1 Tensile and fatigue properties

The presence of inclusions changes the initiation mechanism of tensile and fatigue cracks in wrought superalloys. Under normal circumstances, the sliding zone and grain boundaries interact with each other under tensile and fatigue stresses, and cracks are generated at grain boundaries and in the slip zone [17–19]. When inclusions are present in the alloy, because of the large difference in thermal expansion coefficient and elastic–plastic behavior of the inclusions and matrix, as shown in Table 1, high geometric essential dislocation density, deformation, and strain localization are observed near the inclusions after cyclic loading, leading to the emergence of cracks. However, brittle inclusions on the surface derived from non-metallic

inclusions on the surface or subsurface may fracture under fatigue load, and some inclusions have weak adhesion to the matrix, thus forming small cracks [20].

The inclusion size has been shown to be the main factor affecting the fatigue and fracture properties of nickel-based superalloys [24, 25]. In the low cycle test, the fatigue life of alloys decreases with the increase in inclusion size, as expressed by Eq. (1).

$$l_c = l_0 + \sum_{n=1}^{N_f} \alpha \cdot l_n^\beta \tag{1}$$

where l_c is the critical crack length, μm; l_0 is the initial crack length, that is, the size of the inclusion, μm; N_f is the number of cycles; α and β are constants associated with the alloy; and l_n is the length of the nth crack in the low cycle fatigue test, μm. l_0 is negatively correlated with N_f, that is, for a larger inclusion size, fewer cycles are required to reach the critical crack length.

The type, size, location, and distribution of inclusions as well as the relationship with the orientation of adjacent grains have a comprehensive effect on the initiation and propagation of cracks in wrought superalloys during cyclic fatigue [26, 27]. Figure 2 shows the typical crack path configurations at different types and distributions of inclusions. It has been found that the crack propagation at carbides is relatively small, aggregated carbides lead to very long cracks, crack propagation at coarse carbide does not spread, debunking between the nitride and matrix leads to crack propagation, and crack propagation at the carbides increases during a tensile process [28]. When the size of the grain structure and carbide inclusions are of the same order of magnitude, there is competitive failure between the carbide and grain [29, 30]; when the $\{001\}_{TiN}$ or $\{111\}_{NbC}$ plane is aligned with the $\{111\}_{\gamma\text{-matrix metal grain}}$, interface debonding can be the main factor in crack initiation and propagation [28]. The aggregation effect of inclusions has an important effect on the initiation and propagation of short cracks. Texier et al. [27] observed in
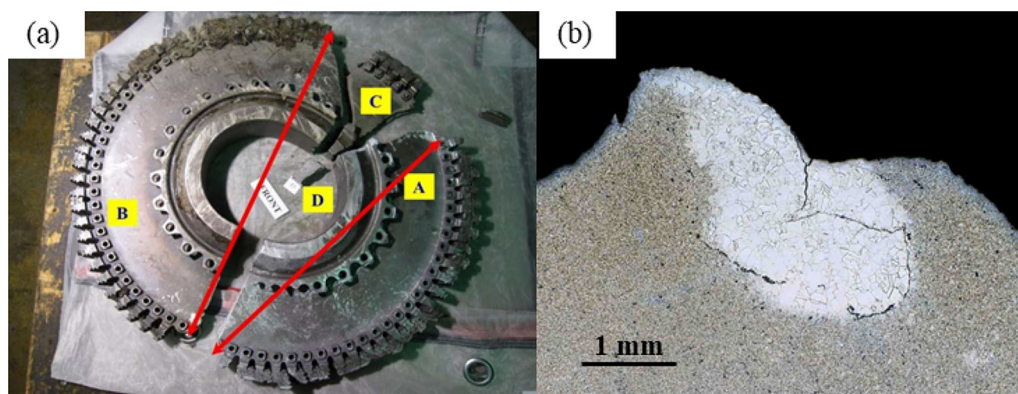

Fig. 1 Failure of Inconel 718 alloy disk for civil aeroengine in 2016. **a** Fatigue failure panel; **b** Al_2O_3–MgO–TiN cluster [16]

Table 1 Mechanical properties and expansion coefficients of inclusions and GH4169 alloy [21–23]

Material	Coefficient of thermal expansion/°C^{-1}	Young modulus/GPa	Poisson's ratio
MgO·Al$_2$O$_3$	8.4×10^{-6}	271	0.26
TiN	9.4×10^{-6}	320	0.19
NbC	6.65×10^{-6}	475.94	0.2345
GH4169	11.8×10^{-6}	199.9	0.3
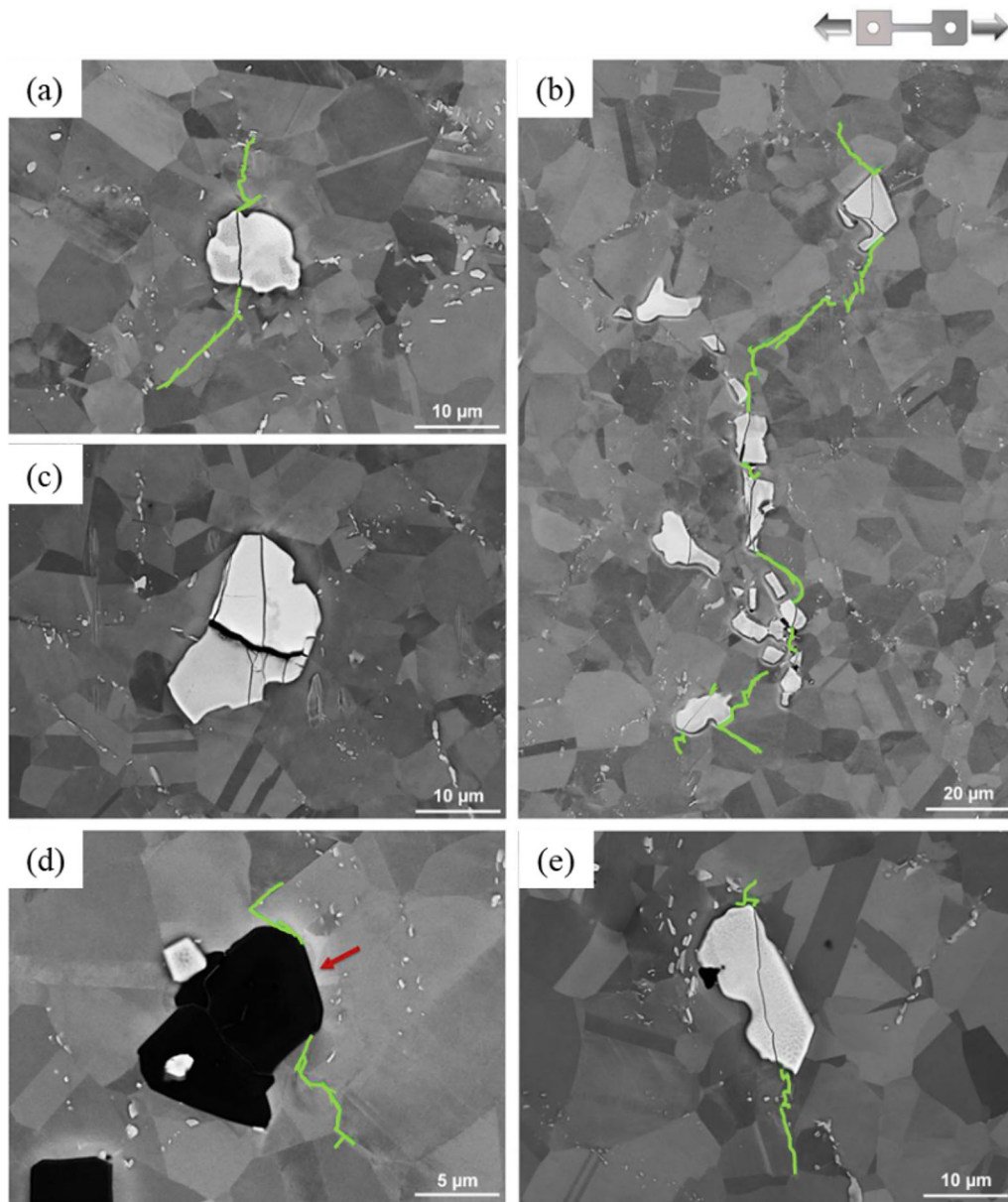
Fig. 2 Typical crack path configurations at different types and distributions of inclusions. **a** Carbide; **b** cluster of carbides; **c** coarse carbide; **d** nitride; **e** carbonitride [28]

an ultra-high cycle fatigue experiment that the starting points of cracks were mainly cluster TiN, separate TiN, grain cluster NbC, and NbC–TiN.

In general, inclusions are necessary but not sufficient conditions for crack initiation and propagation in wrought superalloys. The formation of clusters or large-size

inclusions on the surface and subsurface makes crack initiation and propagation favorable, which can lead to significant deterioration of the tensile and fatigue properties of the alloy. Currently, the effect of inclusion size and distribution on the alloy properties cannot be predicted quantitatively.

2.2 Machinability

In the cutting process of wrought superalloys, hard inclusions damage the cutting edge and flank of the tool and increase the resistance to shear deformation when the alloy is cut, which makes cutting difficult [31, 32]. As shown in Fig. 3, the high-temperature hardness of inclusions (TiC, Ti(C,N), TiN, Al$_2$O$_3$, NbC, etc.) in the wrought superalloy is significantly higher than that of tool materials (WC, Co). Therefore, it is necessary to reduce the inclusion content as much as possible to improve the machinability of the alloy.

3 Types and sources of inclusions

Wrought superalloys are characterized by a high alloying degree, complex preparation process, various raw materials, and complicated types and sources of inclusions. This section summarizes the types and morphologies of inclusions in different grades of inclusions, as shown in Tables 2 and 3.

There are four types of inclusions in wrought superalloys: ceramic oxide inclusions, Al$_2$O$_3$, MgO, etc.; carbide, nitride, sulfide, and other non-metallic inclusions, such as TiC, TiN, Ti(C,N) and CeS; composite inclusions, such as Al$_2$O$_3$·MgO–TiN; and dissimilar metal inclusions, mainly Nb and Cr. Several studies have shown that the amount of
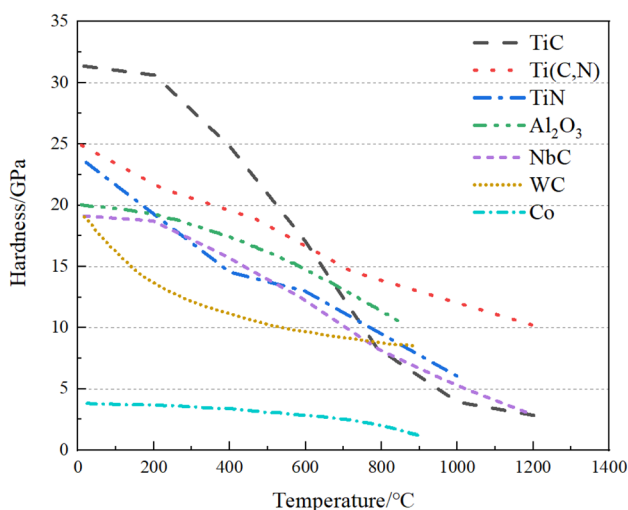

Fig. 3 High-temperature hardness of inclusions and tool materials (WC, Co) in wrought superalloys [31, 33]

nitrides and carbonitrides in alloys is the largest, even one order of magnitude higher than that of oxide inclusions [34, 37]. Inclusions can be divided into endogenous inclusions and foreign inclusions. Endogenous inclusions refer to oxides, nitrides, carbonitrides, sulfides, and composite inclusions formed by O, N, S, C and Al, Ti, Nb during smelting or solidification [42]. Foreign inclusions refer to impurities found in the alloy raw materials, formed by erosion of refractory materials during the smelting process [43, 44], or introduced during electrode treatment processes such as welding [45]. The types and sources of inclusions in wrought superalloys summarized in this section are presented in Fig. 4.

4 Formation of inclusions in wrought superalloys

Because of the variety and high content of active elements in wrought superalloys, the alloy should contain less impurity elements to reduce the formation of inclusions [46, 47]. The complex element composition of wrought superalloys also leads to complex types and formation mechanisms of inclusions. Cockcroft et al. [10] determined the content of each element in the alloy under the control target of "zero inclusion" through thermodynamic calculation of inclusion formation, as summarized in Table 4. In 2004, Mitchell [34] defined "superclean" superalloys from the perspective of nitride and carbide formation in wrought superalloys. It is of great significance to study the formation mechanism of inclusions in wrought superalloys to reach the goal of zero inclusions. However, there remains no perfect theory to explain the formation mechanisms of different types of inclusions in wrought superalloys. Therefore, this section summarizes the research on the phenomenon and mechanism of inclusion formation in wrought superalloys, providing a reference for the establishment of a theoretical system of inclusion formation in wrought superalloys.

4.1 Formation of inclusions in high-temperature melt

Inclusions are in a dynamic thermodynamic equilibrium state in liquid metal, and they mainly exist in a dissolved and precipitated state. The equilibrium concentration product of inclusions is very small because there is sufficient active metal content in the wrought superalloy. The formation of inclusions in the melt is mainly related to the temperature and concentration of the constituent elements. At a certain temperature, when the concentration of the constituent elements is higher than the equilibrium concentration product of the inclusions in the melt, the

Table 2 Types of inclusions in wrought superalloys of different grades

Alloy grade	Melting process	Research method	Type of inclusion	References
Inconel 718	VIM	Metallographic method	TiN, Ti(C,N), MgO, MgS, Al_2O_3, CaO, NbC·TiN, MgO·Al_2O_3·TiN	[10, 34]
GH4169	VIM, VIM + ESR + VAR	Electrolytic extraction, Metallographic method	Oxides, carbonitrides, composite inclusions	[35–37]
ZSGH4169	VIM	–	Ceramic oxides, carbides, sulfides and dissimilar metal inclusions	[18]
GH3625	VIM + ESR	Electrolytic extraction, Metallographic method	(Nb,Ti)(C,N), NbC, (Ti,Nb)N and MgO·Al_2O_3	[38]
GH4700	VIM	Metallographic method	TiN, Al_2O_3·TiN, MgO·Al_2O_3·TiN	[39]
GH4738	VIM + ESR + VAR	Metallographic method	Ti(C,N)–MoS, SiC, Ti(C,N) and oxide	[40]

VIM Vacuum induction melting; ESR electroslag remelting; VAR vacuum arc remelting

inclusions will be precipitated [48]. The general form of the reaction equation and its equilibrium concentration product of inclusions are shown in Eq. (2).

$$r[M] + m[P] = M_rP_m(s)$$
$$K_{M_rP_m} = [w[M] \times f_M]^r \cdot [w[P] \times f_P]^m \quad (2)$$

where $K_{M_rP_m}$ is the reaction equilibrium constant for the reaction of the formation of substance M_rP_m; r and m are constants; $w[M]$ and $w[P]$ represent the mass percent of M (M = Mg, Ti, Ce, Nb, etc.) and P (P = O, N, S, C, etc.) in the alloy melt, respectively; and f_M and f_P represent the activity coefficients of M and P elements in the alloy melt with 1% solution as the standard state, respectively. In a multicomponent solution, the activity coefficient is usually determined using the Wagner method [49, 50]. As wrought superalloys are divided into Fe-, Ni-, and Co-based alloy systems and contain many types of alloying elements, a large amount of thermodynamic data are needed to determine the activity coefficients of alloying elements, among which the activity coefficients of iron-based melt elements are more common [51]. Based on the summary provided by Sigworth et al. [52, 53], the interaction coefficients of O, N, S, and C in nickel-based and cobalt-based alloy melts were supplemented in this paper, providing data support for the calculation of element activity coefficients in nickel-based and cobalt-based alloys, as shown in Table 5.

TiN and Al_2O_3 are typical inclusions in Inconel 718 alloy [35, 61], and their solubility in the alloy is affected by the gas partial pressure, temperature, and element concentration. Figure 5 shows the solubility of Al_2O_3 in Inconel 718. It has been found that 1/3 of the nitrogen in Inconel 718 alloy containing 60×10^{-6} nitrogen exists in the form of nitrides at 1700 K. In addition, the nitride in the melt has a strong aggregation effect, and Mitchell [34] reported a large number of nitride nodulation products during the casting process of superalloys. In Inconel 718 alloy containing 5×10^{-6} oxygen at 1613 K, 2.8×10^{-6}
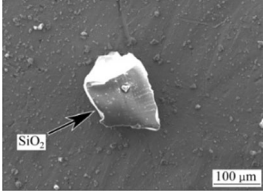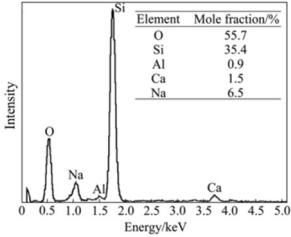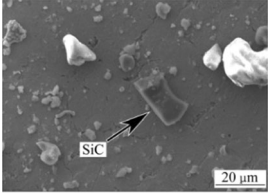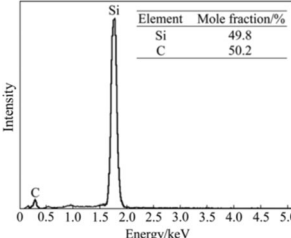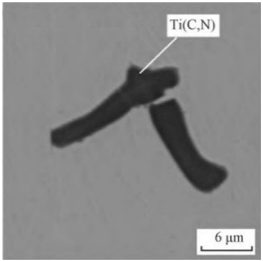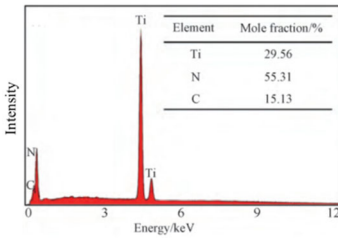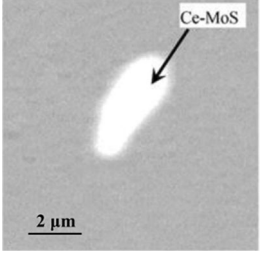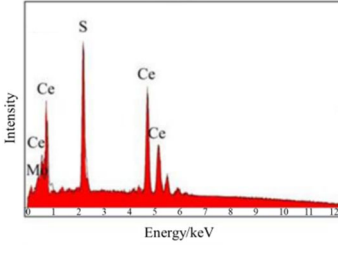
oxygen exists in the form of oxide inclusions and 2.2×10^{-6} oxygen exists in the form of dissolved oxygen [10].

4.2 Formation of inclusions during solidification

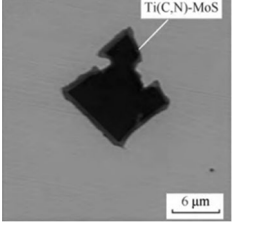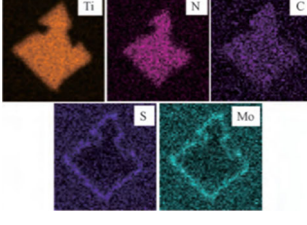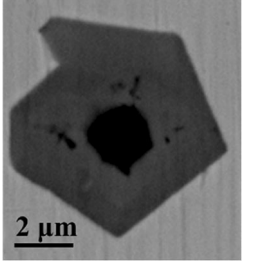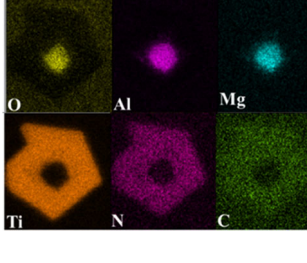According to the classical thermodynamic theory [62, 63], the nucleation of inclusions requires a certain degree of supersaturation. The segregation of alloying elements is one of the key factors that cause the solute concentration on dendrites higher than the nucleation supersaturation of inclusions. The alloy degree of wrought superalloys is high. During the solidification process, the solubility of some solute atoms in the solid and liquid phases is different, resulting in the redistribution of alloying elements, thus resulting in segregation. When the solubility of solute elements in the solid phase is less than that in the liquid phase, the solid–liquid interface will discharge solute into the liquid phase, forming positive segregation, and vice versa. Studies have shown that C, B, Ti, Mo, and Nb are positive segregation elements, while Al is a negative segregation element, and Cr, Co, and Fe are nearly not segregated [64–68]. It can be observed that the positive segregation elements C, Ti, Mo, and Nb in the wrought superalloy correspond precisely to the types of inclusions such as carbides, nitrides, carbonitrides, and sulfides, which verifies that the element segregation is the key factor in the formation of inclusions in the solidification process.

When the concentration of positive segregation elements in the liquid region of the solidification front exceeds the supersaturation required for inclusion nucleation, the inclusions will be precipitated gradually. Wang [35] calculated the precipitation law of the nitride and oxide phases in GH3625 alloy during non-equilibrium solidification using Thermo-Calc software: $L + M_2O_3 \rightarrow L + M_2O_3 + \gamma \rightarrow L + M_2O_3 + \gamma + MN \rightarrow L + M_2O_3 + \gamma + MN + MC(NbC)$. Oxide inclusions were precipitated in the alloy melt, and nitrides were precipitated

Table 3 Types, morphologies, and features of inclusions in wrought superalloys

Type	Morphology	EDS spectrum	Feature	Reference
Oxide			High hardness	[36]
Carbide			High hardness	[36]
Carbonitride			Clustering	[37]
Sulfide			White bright spot	[40]
Composite inclusions			Multilayered	[37]
Composite inclusions			Tangible nuclear center	[41]

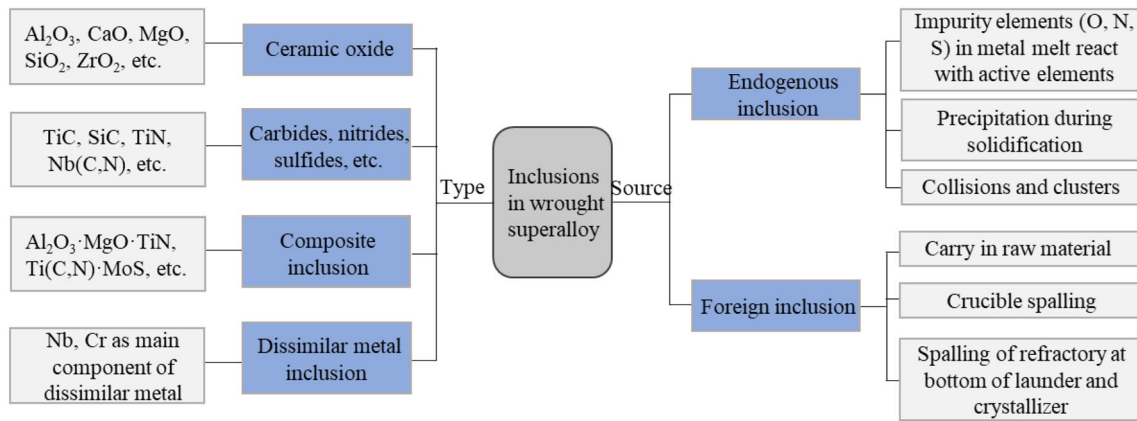EDS Energy dispersive X-ray spectrometry

Fig. 4 Types and sources of inclusions in wrought superalloys

Table 4 Zero inclusion composition for Inconel 718 alloy [10]

Element	S	Mg	N	O
Content/ 10^{-6}	2	5	5	2

during the alloy solidification process. Zhu [69] calculated the nucleation and growth processes of Al_2O_3 and TiN in GH4700 alloy according to the nucleation theory considering the non-equilibrium solidification, as shown in Fig. 6. It is worth noting that the parameters used in the model calculation were mostly measured data on molten steel, which may have resulted in certain deviations when applied to wrought

superalloys. Currently, basic data on the nucleation and growth of inclusions in wrought superalloys are not available, and more basic studies are still needed.

4.3 Formation of composite inclusions and clusters of inclusions

4.3.1 Formation of composite inclusions

The main composite inclusions in wrought superalloy are inclusions with an oxide as the nucleation center and inclusions with a nitride as the nucleation center [10, 34, 70]. Composite inclusions are often large, which seriously affects the mechanical properties of the alloy. According to the nucleation crystal theory proposed by

Table 5 Interaction coefficients e_i^j of O, N, S, and C in nickel-based and cobalt-based alloy melts

e_i^j	Ni-based alloy melt					Co-based alloy melt				
	O	N	S	C	H	O	N	S	C	H
C	− 0.57 (− 1.10 [54])	–	− 1453/T + 0.748 [55]	–	–	− 0.72	–	0.084	–	–
Cr	− 0.20	− 0.101 [56]	0.03	− 0.013	0.0036	− 0.07	− 0.043	–	0.0036	0
Co	− 0.006	− 0.0054	0.007	− 0.001	0.0031	–	–	–	0.0031	–
W	–	− 0.26	–	− 0.001	0.011	–	− 0.007	–	0.011	0.0064
Mo	− 0.024 [54]	− 0.04	0.053	− 0.005	0.011	–	− 0.008	–	0.011	0.0041
Al	− 1.06 [57]	0	0.133	0.027	0.014	–	0.04	–	0.014	0.014
Ti	− 0.51 [54]	− 0.20	0.16	− 0.022	–	–	–	–	–	–
Fe	− 0.029	− 0.02	0.005	0.004	0.0024	− 0.019	− 0.01	− 0.0034	0.0024	0.0014
Nb	–	− 0.075 [54]	–	–	–	–	− 0.042	–	–	0
Mg	–	–	− 9.1 [58]	–	–	–	–	–	–	–
V	− 0.4	− 0.15 [54]	–	− 0.015	0.013	− 0.28	− 0.1	–	0.013	–
B	–	–	–	0.064	–	–	–	–	–	0.09
Zr	− 3.5 [59]	− 0.24	–	–	–	–	–	–	–	–
Ce	–	− 0.55	− 276,228/T + 146 [60]	–0.006	–	–	–	–	–	–

e_i^j Interaction coefficient; i impurity elements, like C, O, N, etc.; j alloying elements in wrought superalloy, including C, Cr, Co, etc.
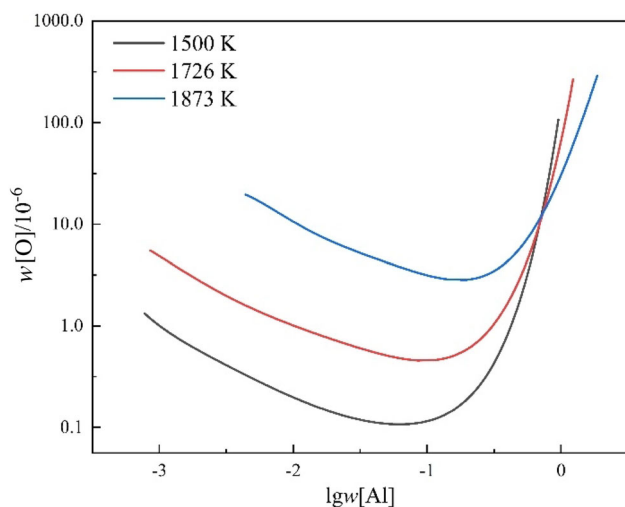
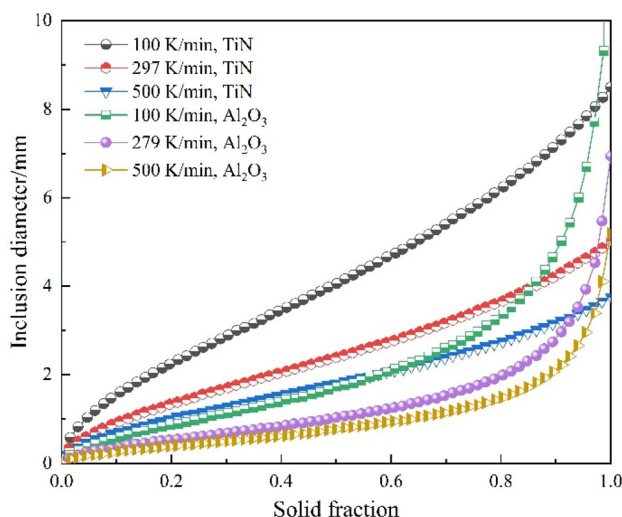Fig. 5 Solubility product of alumina in Inconel 718 alloy [48]

Fig. 6 Change curve of diameters of TiN and Al$_2$O$_3$ with solid-phase fraction [39]

Turnbull and Vonnegut [71], whether the existing phase can act as the heterogeneous nucleation core of the other phase depends mainly on the mismatch between the two phases [47, 72], the wetting angle, the chemical properties, and the surface state. Usually, a smaller mismatch, a smaller wetting angle, and more similar chemical properties are more conducive for heterogeneous nucleation. The misfit between different types of inclusions and TiN and the lattice constant of inclusions are shown in Table 6. It can be observed that the order of dominance of composite inclusions formed by different oxides and titanium nitride is: MgO > MgAl$_2$O$_4$ > Ti$_2$O$_3$ > Al$_2$O$_3$ > Ce$_2$O$_3$.

In addition, the crystal structures of TiC and TiN are face-centered cubic (FCC). The lattice constant of TiC is 0.4320 nm, and that of TiN is 0.4241 nm. The lattice

constant of Ti(C,N) is between that of TiC and TiN [73]. Ti(C,N) is a single compound formed by continuous solution to TiC and TiN. C atoms can be replaced by N atoms in any proportion to form a continuous solid solution Ti(C$_{1-x}$N$_x$) ($0 \leq x \leq 1$).

4.3.2 Clusters of inclusions

The damage of the clusters of inclusions to alloy performance is much greater than that of dispersed inclusions. Inclusion clusters often cause micro-cracks, dirty white spots, and other defects, which reduce the yield of the alloy. Figures 7 and 8 show the clusters of inclusions in wrought superalloys produced by vacuum arc melting and vacuum suspension melting, respectively. The main inclusions in the alloys are oxides, nitrides, and composite inclusions.

In general, Brownian collision, Stokes collision, and turbulent collision of inclusions occur during the melting process, resulting in clusters of inclusions. With vacuum melting of wrought superalloys, the clusters of inclusions are different. Takachio and Nonomura [74] believed that the inclusion aggregation in the VAR furnace results from the formation of a vacuum surface around the inclusion caused by the flow of metal liquid between the inclusions, which changes the interfacial free energy of the inclusion, as shown in Eq. (3). The new inclusions in the molten pool aggregate under the action of interfacial force ΔG.

$$\Delta G = 2\gamma_L \cos \theta \tag{3}$$

where γ_L is the surface tension of the liquid metal; and θ is the contact angle between the solid inclusions and liquid metal. With increasing the contact angle, the probability of liquid metal escaping from the solid inclusion surfaces to form vacuum surfaces increases. According to the surface tension data, Takachio and Nonomura [74] calculated the interfacial free energy changes of Al$_2$O$_3$–Al$_2$O$_3$, TiN–TiN, and Al$_2$O$_3$–TiN in Inconel 718 alloy to be -1.881, 0.926, and -0.477 N/m, respectively. It can be observed that the affinity order for the two inclusions is Al$_2$O$_3$–Al$_2$O$_3$ > Al$_2$O$_3$–TiN > TiN–TiN. However, Al$_2$O$_3$ aggregates are rarely found in the alloy, and there are only a small amount of Al$_2$O$_3$–TiN aggregates and most TiN aggregates. This is because the number of TiN inclusions in the alloy is much higher than that of Al$_2$O$_3$ inclusions.

5 Control of inclusions

To remove, modify, and disperse inclusions in wrought superalloys and reduce the negative effects of inclusions on alloy properties, it is often necessary to optimize the smelting process. Currently, the melting processes of

Table 6 Disregistry data for TiN with various inclusions [46]

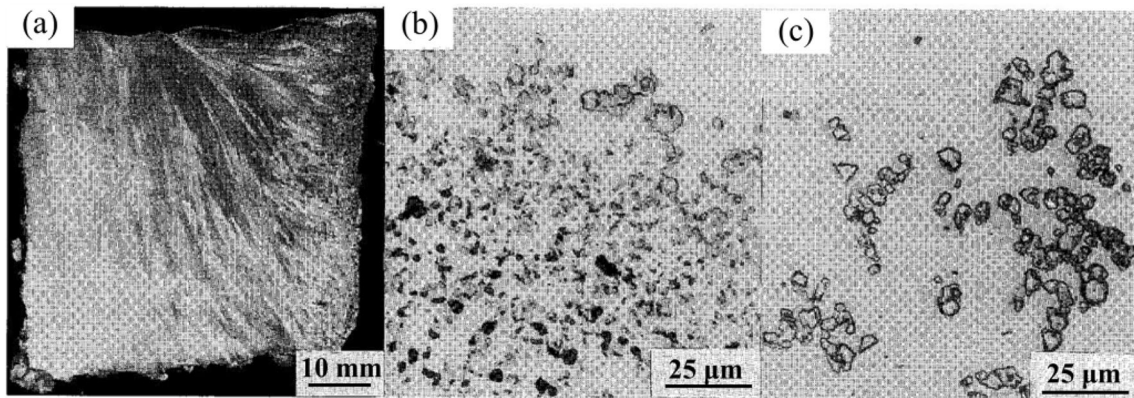| Inclusion	Disregistry with TiN/%	Lattice parameter a at 1811 K/nm
Al_2O_3	17.48	0.4825
Ce_2O_3	29.28	0.3938
MgO	0.053	0.4310
Ti_2O_3	16.17	0.5225
$MgAl_2O_4$	4.88	0.8195
TiN	–	0.4308

Fig. 7 Clusters of inclusions formed by VAR. **a** Macrostructure of ingot top outer; **b** Al_2O_3 (black) + TiN (white) inclusions in shelf; **c** TiN inclusions in shelf [74]
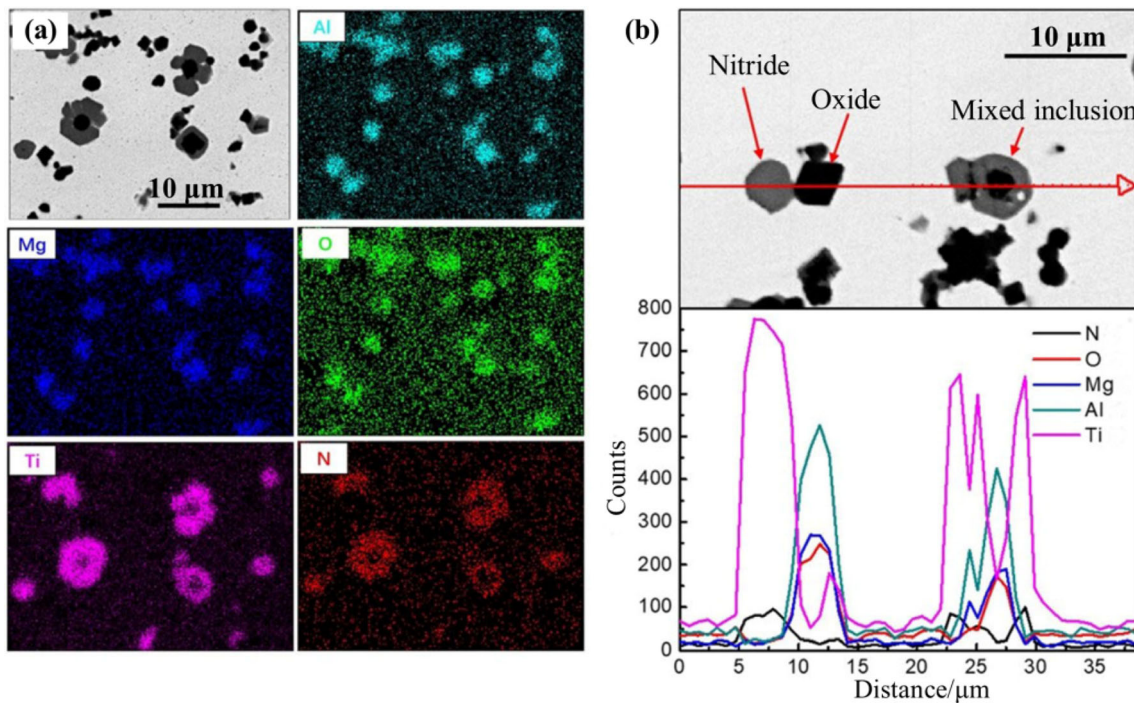

Fig. 8 Clusters of inclusions formed by vacuum suspension melting. **a** Elemental mapping; **b** line-scanning mapping [70]
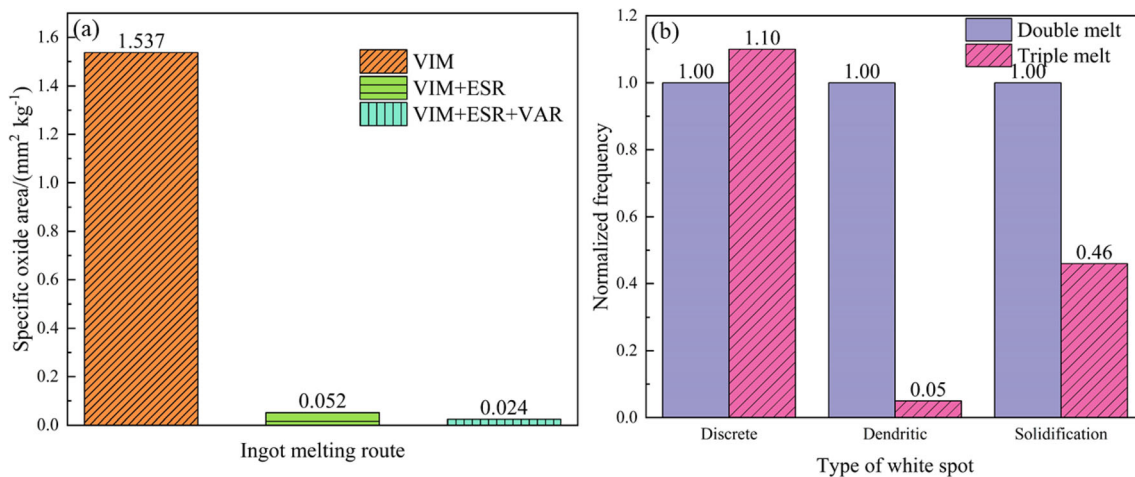
Fig. 9 Comparison of purity of different smelting processes. **a** Specific oxide area; **b** normalized frequency

wrought superalloys include vacuum induction melting, electromagnetic suspension melting (EML), electron beam melting (EBM), protective electroslag remelting (PESR), and vacuum arc remelting [6]. Triple smelting (VIM + PESR + VAR) has been widely used for the smelting of high-purity wrought superalloys and has become an essential melting process for expanding the ingot shape of wrought superalloys [11, 75, 76]. Many studies have shown that triple smelting can significantly reduce the inclusion content and the probability of white spot defects in the alloy [77–79], as shown in Fig. 9a, b. This section summarizes the inclusion control methods of VIM, PESR, and VAR process melting of wrought superalloys, providing a reference for optimizing the triple smelting process.

5.1 Behavior and removal of inclusions in VIM

There are two main ways to remove inclusions in wrought superalloys by VIM. In the first method, the impurity elements in the alloy melt are reduced [80–83] to reduce the generation of endogenous inclusions; however, the removal efficiency of existing inclusions is improved using adsorption [84], flotation [85], and filtration [86]. Currently, the commonly used means of controlling inclusions in VIM under the existing process equipment conditions mainly include the following aspects, as shown in Fig. 10.

1. Control and optimization of the process system of VIM at different stages (feeding, refining, alloying, etc.), as shown in Fig. 10a. A reasonable feeding sequence should be established in the chemical period, and the vacuum degree in the secondary bin should be strictly controlled to maintain consistency with that in the furnace [87]. During the refining period, reasonable vacuum, refining temperature, and refining time are

used [88], and certain amounts of deoxidizer and desulfurizer [84, 89], such as C, Ca, or Ce, are added to further remove [O], [N], [S], and volatile impurity elements in the alloy. The leakage rate of the furnace body should be strictly controlled before and during smelting [90]. It can prevent air leakage into the furnace and increase the partial pressure of oxygen, nitrogen, and hydrogen, resulting in the aggravation of alloy pollution and the increase in inclusions.

2. Optimization of the crucible material. The crucible has two functions in VIM. (1) Decomposition of the crucible occurs to a high vacuum degree [91], as shown in Fig. 10b. (2) A crucible made of a certain material can effectively remove impurity elements [92] and adsorb inclusions [84]. It is noted in Ref. [91] that a MgO crucible has a poor removal effect on large inclusions, a Al_2O_3 crucible has a good removal effect on alloy oxygen and inclusions, and a CaO crucible does not have an obvious removal effect on inclusions but does have a good desulfurization effect [93]. The desulfurization reaction rate is shown in Eq. (4).

$$C_{S,t} = C_{S,0} - \sqrt{\frac{\rho_{CaO}\rho_{Ni}M_S C_{S,fin}Dt}{W_{Ni}^2 M_{CaO}}} \times 10^6 \qquad (4)$$

where t is the desulfurization reaction time, s; $C_{S,0}$, $C_{S,t}$, and $C_{S,fin}$ are the residual S contents in the alloy at the initial, t and final time, respectively, 10^{-6}; ρ_{CaO} and ρ_{Ni} are the densities of the CaO and Ni melts, respectively, g/m^3; D is the effective diffusion coefficient of S, with a measured value of 1.63×10^{-10} $m^2/$s; W_{Ni} is the mass of the nickel-based superalloy melt, g; and M_S and M_{CaO} are the molar mass of S and CaO, respectively, g/mol.

3. Launder and ceramic filter. By placing a slag retaining wall and filter in the flow channel [94, 95], the residence time of high-temperature melts in the flow channel can be prolonged, and the accumulation and floating in inclusions can be promoted. Figure 10c shows the numerical simulation of the structure of the launder and the behavior of inclusions in the launder. In addition, a ceramic filter was placed at the end of the launder [96, 97], which has the advantages of low cost and high removal efficiency. The structure is shown in Fig. 10d. It is worth noting that although the ceramic filter has certain inclusion removal ability, it is not widely used in the smelting of wrought superalloys. This is because the ceramic filter has a significant removal effect on the oxide in the alloy but not on the nitride in the alloy [98]. In addition, the continuous erosion of the ceramic filter will also increase the risk of inclusion formation.

In general, as a primary melting process of wrought superalloys, VIM is the main stage where impurity elements and inclusions are introduced and removed. In addition to the conventional VIM process, various single purification technologies, such as composite molten salt purification agent [99], electromagnetic purification technology [100], and Beijing Institute of Aerial Materials high-quality process [101], are emerging. However, their purification effects still cannot meet the purity requirements for wrought superalloys. Therefore, a secondary or tertiary refining process is often used to further reduce the inclusion content in the alloy.

5.2 Behavior and removal of inclusions in PESR

5.2.1 Inclusion removal mechanism

Several studies [102–105] have shown that the removal behavior of inclusions in PESR mainly occurs in three stages: droplet formation, droplet passing through the slag layer, and metal pool formation, as shown in Fig. 11. During the formation of the droplet on the end of electrode, which is the main stage of removing inclusions, the inclusions have good contact with the slag and a long reaction time. While the droplet is passing through the slag pool, the slag is used to wash the alloy to absorb inclusions; this stage has the characteristics of good contact but the shortest reaction time. During the stage when the inclusions formed during neutralization and solidification of the molten pool float into the slag pool, the contact between the inclusions and slag is poor, but the contact time is long. The removal mechanism, contact time, and specific contact area of the three stages are summarized in Table 7.

In the different PESR processes, the movement, distribution, and removal efficiency of inclusions in the remelting process differ significantly. Because of the characteristics of the PESR system, such as good sealing property, strong melting stability, and complex force of inclusions in the remelting process [105, 106], researchers often use numerical simulation to study the visualization of
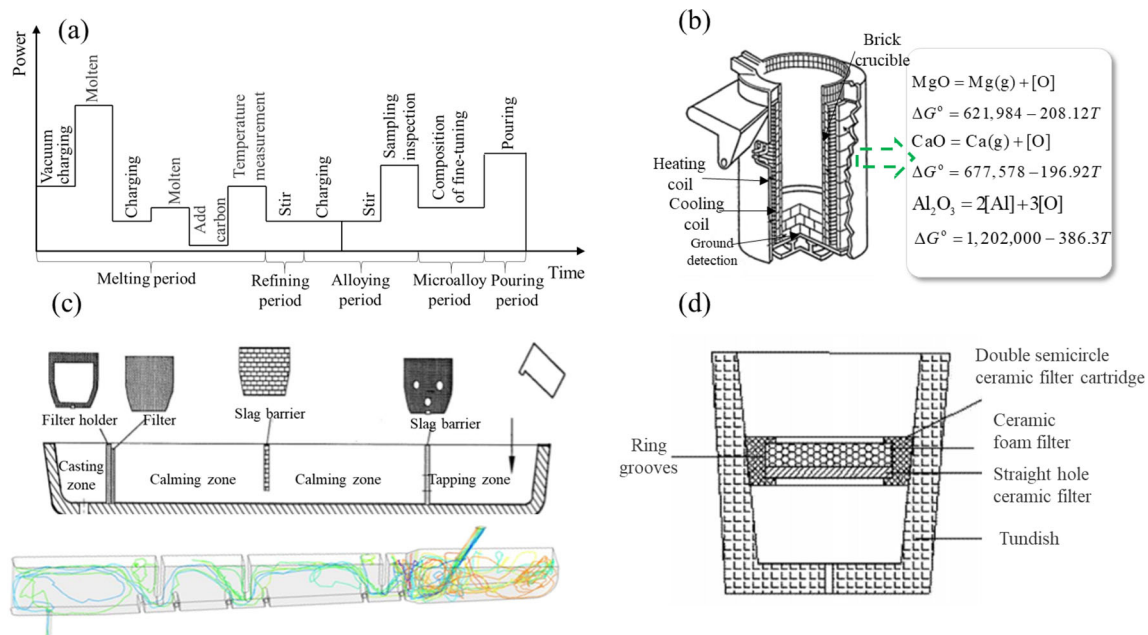

Fig. 10 Purification technology of vacuum induction melting. **a** Process route; **b** crucible; **c** launder; **d** ceramic filter. $\Delta G°$ Standard Gibbs free energy
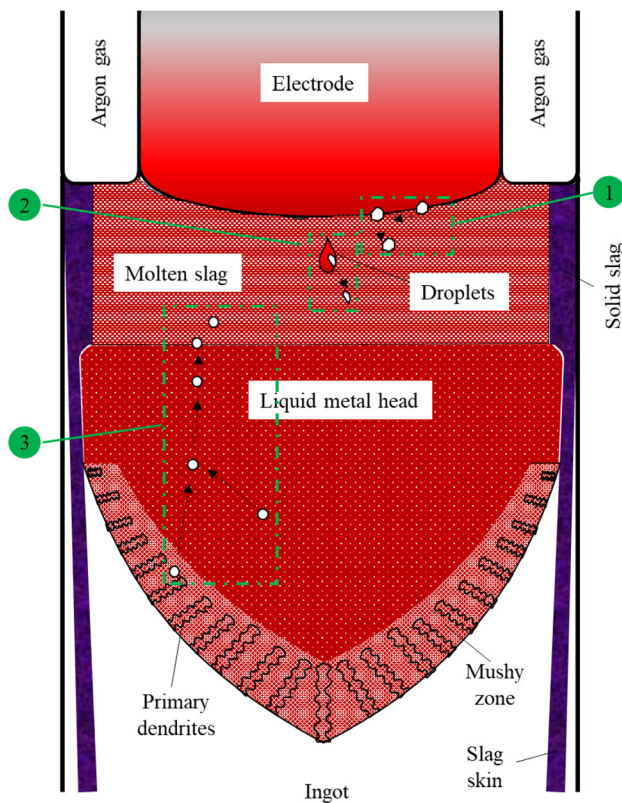
Fig. 11 Schematic diagram of three removal stages of inclusion in PESR process

smelting current are conducive to the removal of inclusions.

It is worth noting that the research on inclusions in ESR is mainly focused on iron and steel materials and serves as a beneficial reference for the optimization of the ESR melting process of wrought superalloys. However, because of the differences in material properties (melting point, viscosity, etc.), inclusion types, remelting process, etc., the process optimization scheme for steel materials cannot be directly applied to the melting process of wrought superalloys and must be further explored according to the smelting characteristics of wrought superalloys.

5.2.2 Modification of inclusions by slag

The composition of slag has a significant effect on the type of inclusions and removal efficiency [103, 111], which has been studied more in other steel grades than in wrought superalloys. This may be because the inclusions in wrought superalloys are mainly nitrides and carbonitrides. Chen et al. [112] showed that the $MgO \cdot Al_2O_3$ inclusion with high melting point and high hardness in GH4169 was modified by adding calcium powder into the slag to form a composite inclusion with an outer coating of $CaO \cdot MgO \cdot Al_2O_3$. The morphology of (Nb,Ti)CN changes from a cluster block or octahedron to a skeleton, as shown in Fig. 13.

5.3 Behavior and removal of inclusions in VAR

5.3.1 Behavior of inclusions

In general, the metallurgical quality of VAR, as the last process of smelting, directly determines the quality of wrought superalloy products. By reasonably controlling the remelting process, the impurities in the electrode can be removed to avoid the accumulation and growth of new inclusions to obtain a high-purity alloy ingot [113]. As shown in Fig. 14, the behavior of inclusions in VAR can be divided into three types: (1) the inclusions in the consumable electrode decompose under high-temperature and high-vacuum conditions; (2) the inclusions generated between the molten pool and dendrite move to the solid–liquid interface at the edge of the molten pool with the flow field of the molten pool and are removed by adsorption;

inclusions in PESR and the removal effect of inclusions under different technological conditions. Wang et al. [107, 108] established a 3D comprehensive mathematical model of ESR and determined the movement trajectory and time distribution of inclusions in a slag pool and metal pool using bidirectional coupling and the Lagrangian method, as shown in Fig. 12a. Kharicha et al. [109] established a two-dimensional mathematical model, which considered the three stages of inclusion movement in ESR (excluding the precipitation of inclusions during solidification) and simulated the distribution of inclusions with different sizes, as shown in Fig. 12b. With the help of MeltFlow software, Du et al. [110] studied the removal effect of inclusions in the ESR process and noted that a larger slag amount and larger

Table 7 Removal mechanism, contact time, and specific contact area of three stages of PESR process [103]

Stage	Removal mechanism	Slag–alloy contact time/s	Contact area ratio/cm^{-1}
①	Motion, dissolve or adsorb	0.23–0.37	15
②	Motion, dissolve or adsorb	0.08–0.11	5.9
③	Float, dissolve or adsorb	–	0.25

Contact area ratio = Contact area between molten alloy and slag/volume of liquid alloy
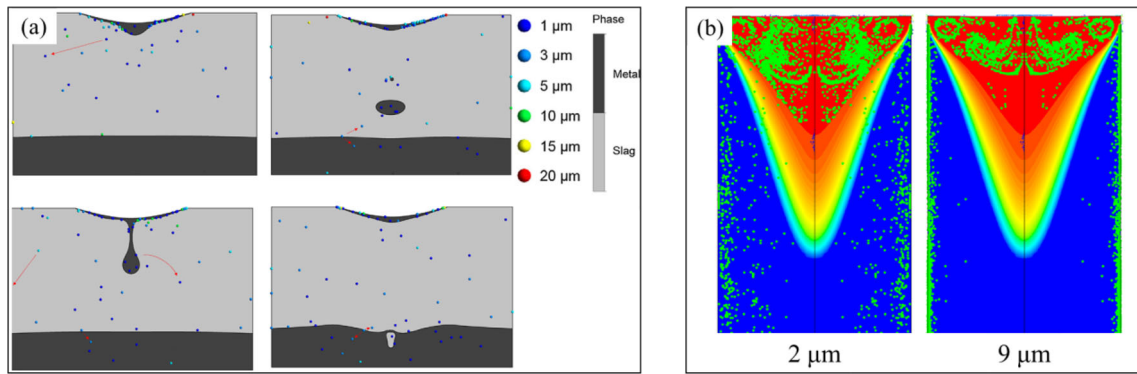
Fig. 12 Visualization of inclusion behavior and distribution in ESR. **a** Inclusions in droplet and slag pool [107]; **b** inclusions in ingots and molten pool [109]
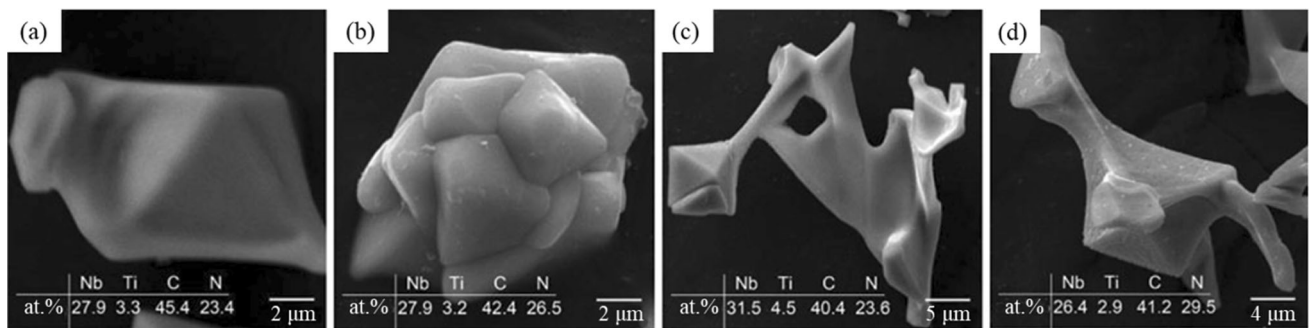

Fig. 13 Three-dimensional SEM images and EDS analysis results of typical precipitates observed in each ESR ingot. **a**, **b** No calcium powder; **c**, **d** added calcium powder [112]
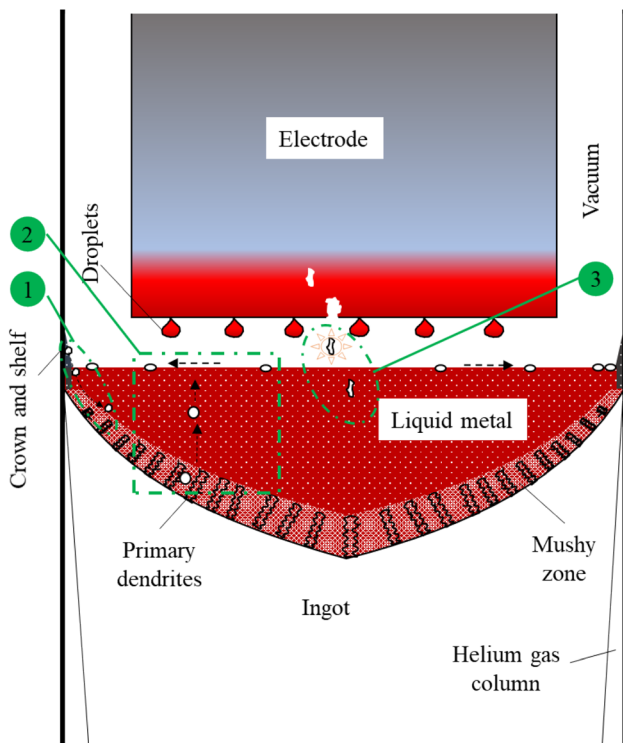

Fig. 14 Behavior of inclusions in VAR

and (3) the metals or inclusions volatilized and splashed at high temperature fall into and remain in the molten pool in the ingot.

The original inclusions in the electrode may cause arc instability and affect the stability of smelting. In the process of metal droplet formation, inclusions gather and grow up inside the droplet and cause tip discharge. The ionization decomposition reaction of inclusions is shown in Eq. (5) [114]. However, it has been noted that the effect of the arc on the removal of inclusions is not obvious.

$$
\begin{aligned}
MC &\rightarrow [M] + [C] \\
MO &\rightarrow [M] + [O] \\
[C] + [O] &\rightarrow CO(g)
\end{aligned}
\tag{5}
$$
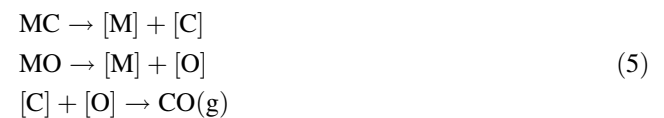
White spots are often produced by solid metals and inclusions falling from the edge shelf and crown of the ingot [3, 115]. Zhang et al. [45] believe that when the diameter of the solid metal and inclusions falling from the edge of the ingot is within 2–3 mm or the thickness is within 4–6 mm, the alloy ingot will not produce white spots.

Under the action of buoyancy and Lorentz force, the inclusions in the molten pool continuously gather at the solid–liquid interface at the edge of the ingot, resulting in a
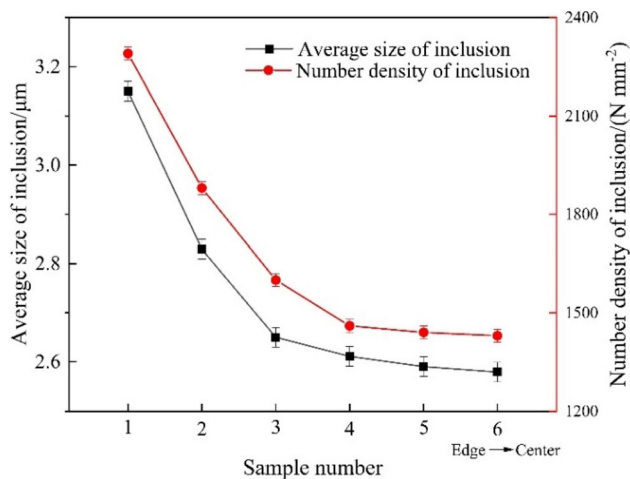
Fig. 15 Radial distribution of inclusions in VAR ingot [116]

decrease in the number and size of inclusions along the radial direction (center to edge), as shown in Fig. 15.

5.3.2 Factors affecting inclusion removal

The unique characteristics of vacuum arc melting equipment provide inherent advantages for purification melting: (1) with no refractory, the probability of foreign inclusions is almost zero; (2) high vacuum degree and extremely high arc temperature (2400–2700 K) create good conditions for the volatilization and removal of impurity gas and impurity elements [117]; (3) helium and cooling water greatly improve the cooling rate of the ingot, resulting in smaller endogenous inclusions; (4) under the action of Lorentz force, the inclusions in the molten pool move to the solid–liquid interface at the edge of the ingot to achieve the removal effect.

The operation conditions such as the vacuum degree, current intensity, and filling ratio are the key factors affecting the removal of inclusions in vacuum consumptive melting. As shown in Fig. 16a–c, with increasing current and vacuum degree, the number of inclusions decreased significantly, whereas the effect of the filling ratio on inclusion removal was not obvious. However, Takachio and Nonomura [74] reported that the probability of inclusion aggregation to produce white spots decreased significantly with increasing VAR filling ratio, as shown in Fig. 16d. This may be due to the reduction of volatiles and spatter at the crown as the filling ratio increases, which reduces the probability of particles falling from the ingot head. In general, high vacuum degree, high current intensity, and high filling ratio are conducive to the removal of inclusions. However, it remains to be further explored how to develop an accurate remelting process for different ingot types and different grades of wrought superalloys.

6 Conclusions: restrictive problems and development trends

The presence of inclusions results in deterioration of the mechanical properties and processability of the alloy, especially the cluster inclusions, which seriously reduce the stability of the alloy properties. Due to the special application field of wrought superalloy, it is generally considered that it will be better to possibly lower the content of inclusions in superalloy. Currently, the problems of alloy quality caused by inclusions have been basically solved by improving the triple smelting process in the USA, but the related technology is still in the phase of confidentiality. However, the improvement of triple smelting process in China is still in the exploratory stage, and the content of inclusions in wrought superalloy is unstable. To achieve the goal of "zero inclusion" control, more in-depth theoretical research is needed:

1. Deep removal technology of impurity elements. The fundamental way to achieve the goal of "zero inclusion" is to further reduce the impurity elements in the wrought superalloy and control their content below the equilibrium concentration product of inclusions.
2. Basic research on the thermodynamics and kinetics of inclusion formation. Because of the high alloying characteristics of wrought superalloys and the incomplete thermodynamic data for multicomponent high-temperature melts in Ni-based and Co-based alloys, it is a challenge to study the formation process of inclusions.
3. The behavior of inclusions at the directional solidification front. The solidification process of PESR and VAR is similar to directional solidification, and the mechanism of inclusion formation and removal has not been reported. Therefore, it is of great significance to study the removal of inclusions and the adhesion of inclusions at the solidification front in the directional solidification process of wrought superalloys.
4. Accurate prediction and control of dirty white spots. The formation of white spots resulting from inclusion aggregation in VAR remains an important problem in the stable production of wrought superalloys. Therefore, it is necessary to study the motion and dissolution mechanism of inclusions in vacuum consumptive remelting and predict the distribution of inclusions in vacuum consumptive ingots. Furthermore, the VAR process can be optimized to fundamentally solve the problem of dirty white spots caused by inclusions.
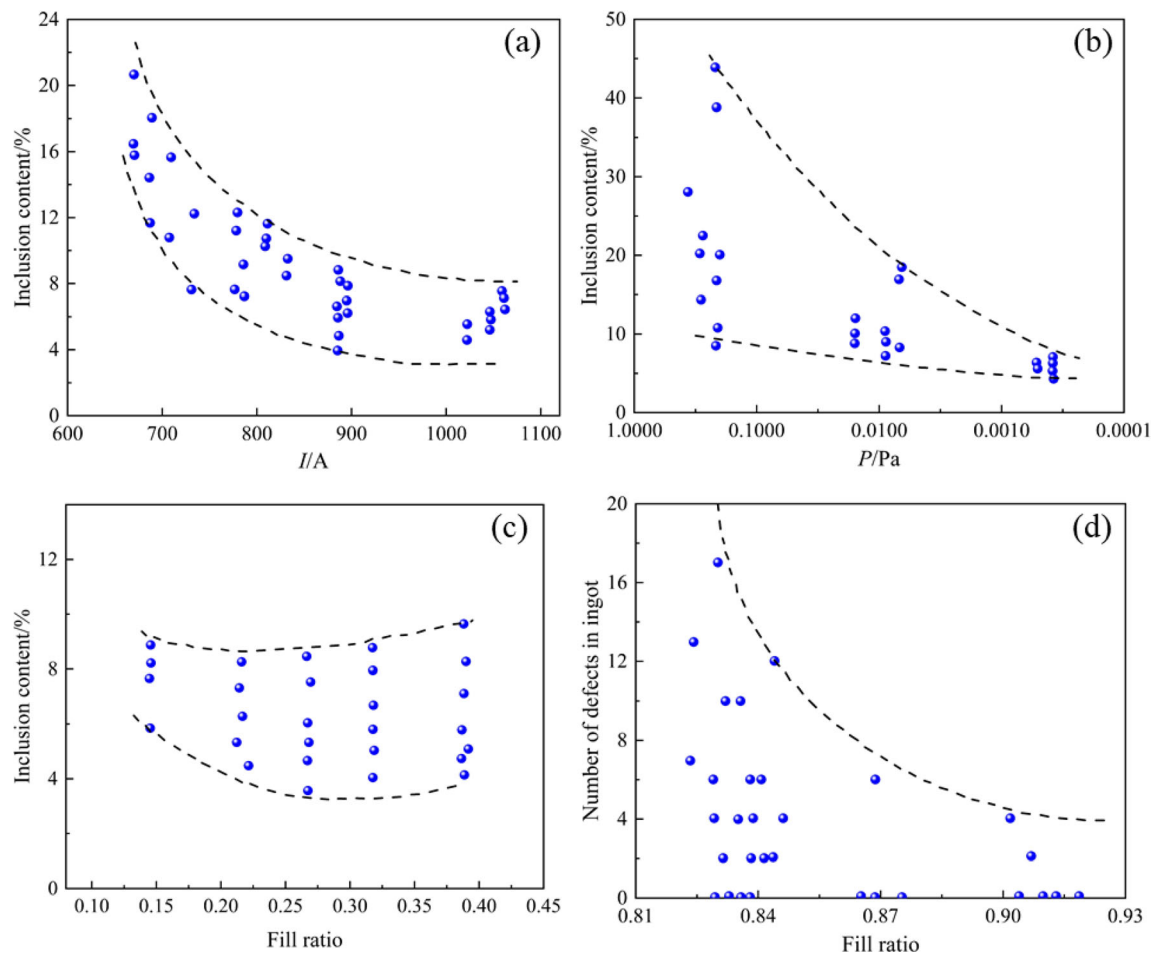
Fig. 16 Effect of vacuum degree (**a**), current intensity (**b**) and filling ratio (**c**) on inclusion or defect content (**d**) [74, 118]

References

[1] Z.J. Tang, T.M. Guo, Y. Fu, Z. Hui, C.S. Han, Metal World (2014) No. 1, 36–40.

[2] J.R. Li, J.C. Xiong, D.Z. Tang, Advanced high temperature structural materials and technology, National Defense Industry Press, Beijing, China, 2012.

[3] Z.Y. Zhong, J.Y. Zhuang, J. Iron Steel Res. 15 (2003) No. z1, 1–9.

[4] J.H. Du, X.D. Lv, J.X. Dong, W.R. Sun, Z.N. Bi, G.P. Zhao, Q. Deng, C.Q. Cui, H.P. Ma, B.J. Zhang, Acta Metall. Sin. 55 (2019) 1115–1132.

[5] D.X. Wen, Y.C. Lin, H.B. Li, X.M. Chen, J. Deng, L.T. Li, Mater. Sci. Eng. A 591 (2014) 183–192.

[6] Y. Zhang, P.H. Li, C.L. Jia, T. Wang, X.X. Li, Y. Li, Mater. Rep. 32 (2018) 1496–1506.

[7] J.K. Tien, J.C. Borofka, M.E. Casey, JOM 38 (1986) 13–17.

[8] A. Mitchell, S.L. Cockcroft, C.E. Schvezov, A.J. Schmalz, J.N. Loquet, J. Fernihough, High Temp. Mater. Process 15 (1996) 27–40.

[9] C.E. Shamble, D.R. Chang, J.A. Corrado, in: Proceedings of the Fifth International Symposium on Superalloys, TMS-AIME, Warrendale, PA, USA, 1984, pp. 509–519.

[10] S.L. Cockcroft, T. Degawa, A. Mitchell, D.W. Tripp, A. Schmalz, in: S.D. Antolovich, R.W. Stusrud, R.A. MacKay, D.L. Anton, T. Khan, R.D. Kissinger, D.L. Klarstrom (Eds.), Superalloys 1992, The Minerals, Metals, and Materials Society (TMS), San Diego, USA, 1992, pp. 577–586.

[11] G.S. Chen, F.J. Liu, Q.Z. Wang, Z.X. Wang, Z.G. Wei, J. Iron Steel Res. 23 (2011) No. S2, 134–137.

[12] R. Schafrik, R. Sprague, Key Eng. Mater. 380 (2008) 113–134.

[13] B.J. Zhang, S. Huang, W.Y. Zhang, Q. Tian, S.F. Chen, Acta Metall. Sin. 55 (2019) 1095–1114.

[14] C.F. Miller, G.W. Simmons, R.P. Wei, Scripta Mater. 44 (2001) 2405–2410.

[15] R. Jiang, D.W. Ji, H.C. Shi, X.T. Hu, Y.D. Song, B. Gan, Mater. Sci. Technol. 35 (2019) 1265–1274.

[16] NTSB, Powerplant group chairman's factual report, National Transportation Safety Board, Washington, USA, 2017.

[17] L. Wang, Y.M. Liu, G. Chen, J. Liu, Materials for Mechanical Engineering 43 (2019) 45–49.

[18] B. Meng, W.L. Guo, C.M. Yu, Chinese Journal of Materials Research 21 (2007) 30–33.

[19] R. Bandyopadhyay, M.D. Sangid, Acta Mater. 177 (2019) 20–34.

[20] L. Zhu, Z.R. Wu, X.T. Hu, Y.D. Song, Fatigue Fract. Eng. Mater. Struct. 39 (2016) 1150–1160.

[21] N. Rathod, S.D. Gupta, S.K. Gupta, P.K. Jha, Solid State Phenom. 171 (2011) 67–77.

[22] D. Brooksbank, K.W. Andrews, J. Iron Steel Inst. 206 (1968) 595–599.

[23] C. Gu, Microstructure fatigue life prediction model based on the effect of inclusions in bearing steel, University of Science and Technology Beijing, Beijing, China, 2019.

[24] T. Denda, P.L. Bretz, J.K. Tien, Metall. Trans. A 23 (1992) 519–526.

[25] C. Wang, Y.P. Zeng, X.S. Xie, J. Univ. Sci. Technol. Beijing 31 (2009) 557–562.

[26] X. Huang, H. Yu, M. Xu, Y. Zhao, Int. J. Fatigue 42 (2012) 153–164.

[27] D. Texier, J. Cormier, P. Villechaise, J.C. Stinville, C.J. Torbet, S. Pierret, T.M. Pollock, Mater. Sci. Eng. A 678 (2016) 122–136.

[28] D. Texier, J.C. Stinville, M.P. Echlin, S. Pierret, P. Villechaise, T.M. Pollock, J. Cormier, Acta Mater. 165 (2019) 241–258.

[29] N. Späth, V. Zerrouki, P. Poubanne, J.Y. Guedou, in: E.A. Loria (Eds.), CBMM North America, Inc. Superalloys 718, 625, 706 and Various Derivatives, TMS, Warrendale, USA, 2001, pp. 173–183.

[30] F. Alexandre, R. Piques, S. Deyber, A. Pineau, High temperature creep-fatigue crack initiation in 718-DA Ni based superalloy, in: Fract. Mech. beyond 2000 ECF14, Cracow (Poland), 2002.

[31] P. Hoier, A. Malakizadi, P. Stuppa, S. Cedergren, U. Klement, Wear 400–401 (2018) 184–193.

[32] L.H. Xu, Z.F. Jiang, J.E. Ståhl, Modern Manufacturing Engineering (2010) No. 2, 91–94.

[33] P.C. Jindal, A.T. Santhanam, U. Schleinkofer, A.F. Shuster, Int. J. Refract. Met. Hard Mater. 17 (1999) 163–170.

[34] A. Mitchell, High Temp. Mater. Process. 24 (2005) 101–109.

[35] W. Wang, Investigation of inclusion and purification in alloy GH3625, Lanzhou University of Technology, Lanzhou, China, 2016.

[36] Z.J. Tang, T.M. Guo, S.Z. Kou, Y. Fu, S. Jin, The Chinese Journal of Nonferrous Metals 25 (2015) 2403–2413.

[37] H.B. Zheng, S.F. Yang, Z.Y. Chen, J.S. Li, China Metall. 28 (2018) No. S1, 41–45.

[38] J.L. Qu, S.F. Yang, Z.Y. Chen, J.H. Du, J.S. Li, D. Wang, Materials 12 (2019) 1852.

[39] Y. Wang, L. Zeng, H.J. Miao, L. Li, W.H. Hao, Materials Science and Technology 21 (2013) 122–128.

[40] Z.Y. Chen, S.F. Yang, J.L. Qu, J.S. Li, A.P. Dong, Y. Gu, Materials 11 (2018) 1838.

[41] D. Wang, Study on precipitation and gradual change of inclusions in GH4169 superalloy during triple-smelting, University of Science and Technology Beijing, Beijing, China, 2020.

[42] C. Schröder, U. Fischer, A. Schmidt, G. Schmidt, O. Volkova, C.G. Aneziris, Adv. Eng. Mater. 19 (2017) 1700146.

[43] X. Ren, J. Xiao, World Nonferrous Metals (2018) No. 10, 18–21.

[44] Y.T. Ding, W. Wang, H.F. Li, T.B. Guo, Y. Hu, J.J. Liu, Rare Metal Mat. Eng. 47 (2018) 687–691.

[45] W. Zhang, P.D. Lee, M. Mclean, in: T.M. Pollock (Eds.), Proceedings of the 9th Int. Symp. on Superalloys, TMS, Warrendale, USA, 2000, pp. 29–37.

[46] J.H. Park, Y.B. Kang, Metall. Mater. Trans. B 37 (2006) 791–797.

[47] J.S. Park, C.H. Lee, J.H. Park, Metall. Mater. Trans. B 43 (2012) 1550–1564.

[48] H. Itoh, M. Hino, S. Ban-Ya, Metall. Mater. Trans. B 28 (1997) 953–956.

[49] X.Y. Ding, W.Z. Wang, P. Fan, Metall. Mater. Trans. B 30 (1999) 271–277.

[50] Q.Z. Le, X.J. Zhang, J.Z. Cui, G.M. Lu, Acta Metall. Sin. 39 (2003) 35–42.

[51] X.H. Huang, Principle of iron and steel metallurgy, Metallurgical Industry Press, Beijing, China, 1981.

[52] G.K. Sigworth, J.F. Elliott, G. Vaughn, G.H. Geiger, Can. Metall. Quart. 16 (1977) 104–110.

[53] G.K. Sigworth, J.F. Elliott, Can. Metall. Quart. 15 (1976) 123–127.

[54] Y. Haruna, Removal of inclusions from cast superalloy revert, University of British Columbia, Vancouver, Canada, 1994.

[55] W.V. Venal, G.H. Geiger, Metall. Trans. 4 (1973) 2567–2573.

[56] H. Wada, R.D. Pehlke, Metall. Trans. B 8 (1977) 443–450.

[57] S.W. Cho, H. Suito, Metall. Mater. Trans. B 26 (1995) 249–256.

[58] C.H. Wang, Q.Y. Han, Acta Metall. Sin. 24 (1988) 524–526.

[59] A.A. Aleksandrov, V.Y. Dashevskii, Russ. Metall. 2016 (2016) 832–838.

[60] L.M. Wang, T. Du, J. Iron Steel Res. 1 (1989) No. 1, 15–20.

[61] J.J. Ruan, N. Ueshima, K. Oikawa, J. Alloy. Compd. 737 (2018) 83–91.

[62] G.H. Gulliver, J. Inst. Met. 9 (1913) 120–157.

[63] E. Kozeschnik, Metall. Mater. Trans. A 31 (2000) 1682–1684.

[64] X.F. Yan, J.X. Dong, Z.X. Shi, C.H. Duan, Rare Metal Mat. Eng. 48 (2019) 3183–3189.

[65] L. Wang, Z.X. Xiao, L. Zhao, Y.G. Bai, F.X. Yin, Foundry Technology 41 (2020) 9–14.

[66] Y. Zhang, X.X. Li, K. Wei, J.H. Wei, T. Wang, C.L. Jia, Z. Li, Z.Q. Ma, Acta Metall. Sin. 56 (2020) 1123–1132.

[67] B.Y. Zhong, L. Wang, M.C. Zhang, J.X. Dong, J. Univ. Sci. Technol. Beijing 30 (2008) 760–764.

[68] L. Wang, B.Y. Zhong, J.X. Dong, M.C. Zhang, Rare Metal Mat. Eng. 36 (2007) 2104–2108.

[69] H.X. Zhu, Foundry Technology 36 (2015) 15–17.

[70] X.Y. Gao, L. Zhang, Y.F. Luan, X.W. Chen, X.H. Qu, JOM 72 (2020) 3247–3255.

[71] D. Turnbull, B. Vonnegut, Ind. Eng. Chem. 44 (1952) 1292–1298.

[72] B.L. Bramfitt, Metall. Trans. 1 (1970) 1987–1995.

[73] M.L. Gan, Synthesis of TiN, TiC and Ti(C,N) and application in carbon brick, Wuhan University of Science and Technology, Wuhan, China, 2006.

[74] K. Takachio, T. Nonomura, ISIJ Int. 36 (1996) S85–S88.

[75] Y.S. Xu, Y.Q. Wu, X.X. Wu, X.F. Chen, X.H. Gao, Q.J. Wan, Modern Manufacturing Technology and Equipment (2019) No. 7, 169–170.

[76] J.H. Du, Q. Deng, J.L. Qu, X.D. Lv, M.Q. Wang, Z.N. Bi, T.H. Xu, J. Iron Steel Res. 23 (2011) No. S2, 130–133.

[77] E.E. Brown, J.E. Stulga, L. Jennings. R.W. Salkeld, in: T.K. Tien (Eds.), Proceedings of the Fourth International Symposium, ASM, PA, USA, 1980, pp. 159–168.

[78] A. Mitchell, Mater. Sci. Eng. A 263 (1999) 217–223.

[79] J.M. Moyer, L.A. Jackman, C.B. Adasczik, R.M. Davis, R. Forbes-Jones, in: E.A. Loria (Eds.), Superalloys 718, 625, 706 and Various Derivatives, TMS, Warrendale, USA, 1994, pp. 39–48.

[80] Z.H. Jiang, X.F. Zhang, F.B. Liu, W. Gong, Iron and Steel 52 (2017) No. 9, 1–10.

[81] V.V. Sidorov, P.G. Min, Russ. Metall. 2014 (2014) 982–986.

[82] J. Alexander, Mater. Sci. Technol. 1 (1985) 167–170.

[83] Y.J. Yang, Z.G. Wang, Y.C. Zhang, X.L. Yang, P. Zhang, J. Iron Steel Res. 23 (2011) No. S2, 5–8.

[84] D. Li, F. Cosandey, G.E. Maurer, R. Foote, J.K. Tien, Metall. Trans. B 13 (1982) 603–611.

[85] S.W. Cho, H. Suito, Metall. Mater. Trans. B 25 (1994) 5–13.

[86] J.L. Qu, X.L. Zhang, S.F. Yang, Y. Gu, Y. Tao, Powder Metallurgy Industry 30 (2020) No. 5, 1–11.

[87] J.P. Niu, K.N. Yang, T. Jin, X.F. Sun, H.R. Guan, Z.Q. Hu, Acta Metall. Sin. 37 (2001) 943–946.

[88] N. An, J.J. Tian, Z.R. Li, Y.J. Niu, C.W. Li, H.W. Liu, J.Y. Xu, A vacuum induction melting method for reducing nitrogen content in superalloys, China, CN105238934A, 2015.

[89] Q.L. Li, H.R. Zhang, M. Gao, J.P. Li, T.X. Tao, H. Zhang, Int. J. Miner. Metall. Mater. 25 (2018) 696–703.

[90] X.H. Liu, C.H. Xu, X.F. Zheng, Vacuum smelting, Chemical Industry Press, Beijing, China, 2013.

[91] H.Y. Zhao, J. Iron Steel Res. 24 (2012) No. 1, 19–24.

[92] K. Takahashi, K. Utagawa, H. Shibata, S.Y. Kitamura, N. Kikuchi, Y. Kishimoto, ISIJ Int. 52 (2012) 10–17.

[93] Y. Kishimoto, S. Utada, T. Iguchi, Y. Mori, M. Osawa, T. Yokokawa, T. Kobayashi, K. Kawagishi, S. Suzuki, H. Harada, Metall. Mater. Trans. B 51 (2019) 293–305.

[94] M. Hohmann, S. Jönsson, Vacuum 41 (1990) 2173–2176.

[95] Y.H. Wang, J.Y. Li, S.F. Yang, J.S. Li, China Metall. 30 (2020) No. 7, 23–27.

[96] G.R. Brazer, P.M. Curran, J.S. Erickson. Method of cleaning nickel alloy by filtering, USA, US3869282 A, 1975.

[97] F. Chen, X. Huang, Y. Wang, Y. Zhang, Z. Hu, Mater. Lett. 34 (1998) 372–376.

[98] X.Z. Guo, J.X. Dong, Y.H. Hu, X.S. Xie, J. Univ. Sci. Technol. Beijing 21 (1999) 245–247.

[99] Z.C. Peng, F.Q. Xie, X.Q. Wu, J. Zhang, Journal of Materials Engineering (2013) No. 8, 11–15.

[100] W.Z. Jin, W. Zhang, T.J. Li, G.M. Yin, Chin. J. Vac. Sci. Technol. 31 (2011) 589–593.

[101] Z.L. Gui, C.X. Wu, C.Q. Sun, Q.J. Li, X.Y. Dai, Journal of Materials Engineering (2002) No. 3, 20–23.

[102] Y.W. Dong, Z.H. Jiang, Y.L. Cao, A. Yu, H. Dong, Metall. Mater. Trans. B 45 (2014) 1315–1324.

[103] X. Gen. Z.H. Jiang, F.B. Liu, L.K. Liang, Iron and Steel 44 (2009) No. 12, 42–45.

[104] Z.B. Li, W.H. Zhuo, Y.D. Li, Iron and Steel 15 (1980) No. 1, 20–26.

[105] T.J. Wen, L.F. Zhang, China Metall. 28 (2018) No. S1, 34–40.

[106] S.F. Yang, J.S. Li, C. Liu, L.Y. Sun, H.B. Yang, Metall. Mater. Trans. B 45 (2014) 2453–2463.

[107] Q. Wang, R.T. Wang, Z. He, G.Q. Li, B.K. Li, H.B. Li, Int. J. Heat Mass Transfer 125 (2018) 1333–1344.

[108] R.T. Wang, G.Q. Li, Q. Wang, Y. Liu, B.K. Li, J. Iron Steel Res. 30 (2018) 104–112.

[109] A. Kharicha, E. Karimi-Sibaki, M. Wu, A. Ludwig, J. Bohacek, Steel Res. Int. 89 (2018) 1700100.

[110] G. Du, J. Li, Z.B. Wang, ISIJ Int. 58 (2018) 78–87.

[111] Y. Liu, Z. Zhang, G.Q. Li, Q. Wang, L. Wang, B.K. Li, Steel Res. Int. 88 (2017) 1700058.

[112] X.C. Chen, C.B. Shi, H.J. Guo, F. Wang, H. Ren, D. Feng, Metall. Mater. Trans. B 43 (2012) 1596–1607.

[113] Z.Z. Wang, D.H. Zhou, X. Jin, G.S. Chen, J. Iron Steel Res. 15 (2003) No. z1, 338–343.

[114] H.T. Zhu, X.H. L, B.M. Zhu, Y.J. Yang, X.C. Bai, X.M. Zhang, in: Zcademic Committee of the Superalloys, CSM (Eds.), The 14th Superalloy Annual Conference, Huangshi, China, 2019, pp. 421–423.

[115] W. Zhang, P.D. Lee, M. McLean, Metall. Mater. Trans. A 33 (2002) 443–454.

[116] H.H. Kong, S.F. Yang, J.L. Qu, J.H. Du, Y.C. Huang, Acta Aeronaut. Astronaut. Sin. 41 (2020) No. 4, 304–311.

[117] P.C.L. Pfeil, L.B. Griffiths, J. Nucl. Mater. 1 (1959) 244–248.

[118] G.D. Zhang, J.J. Liu, Z.Q. Chen, J.Y. Liu, W.D. Hua, X.S. Wang, W.F. Zhang, Y.Q. Wang, Journal of Tsinghua University (Science and Technology) 12 (1965) No. 1, 21–32.